IEEE Access
Multidisciplinary | Rapid Review | Open Access Journal

Received 9 May 2024, accepted 2 June 2024, date of publication 6 June 2024, date of current version 13 June 2024.

*Digital Object Identifier 10.1109/ACCESS.2024.3410675*

RESEARCH ARTICLE

# Joint State of Charge and State of Health Estimation Using Bidirectional LSTM and Bayesian Hyperparameter Optimization

**PANAGIOTIS ELEFTHERIADIS[1], (Student Member, IEEE), SPYRIDON GIAZITZIS[1], JULIA KOWAL[2], (Member, IEEE), SONIA LEVA[1], (Senior Member, IEEE), AND EMANUELE OGLIARI[1], (Member, IEEE)**

[1]Politecnico di Milano, 20127 Milan, Italy
[2]Institute of Energy and Automation Technology, Technische Universität Berlin, 10587 Berlin, Germany

Corresponding author: Panagiotis Eleftheriadis (panagiotis.eleftheriadis@polimi.it)

This work was supported by MOST –Sustainable Mobility Center through the European Union Next-GenerationEU Piano Nazionale di Ripresa e Resilienza (PNRR)–MISSIONE 4 COMPONENTE 2, INVESTIMENTO 1.4–D.D. 1033 17/06/2022, under Grant CN00000023.

**ABSTRACT** In this study, a novel Machine learning-based method for the joint State of Charge and State of Health estimation of Lithium Batteries that tackle real-world applications and with Bayesian Hyperparameter optimization is proposed. The estimated State of Health is used as an input for State of Charge estimation, considering battery degradation. The accuracy and computational cost of the proposed method are compared with the other state-of-the-art Machine Learning models. For the most promising solutions, an in-depth analysis on factors affecting the estimation accuracy is performed. To facilitate further research, a new battery dataset was created using extended dynamic driving cycles, encompassing a wide range of temperature conditions and aging stages. This dataset is publicly available online to support model development and comparative testing by the scientific community. The proposed solution achieves low estimation errors for the whole first life of Lithium Batteries for dynamic applications while providing valuable insights into its applicability and effectiveness in battery energy storage systems.

**INDEX TERMS** BiLSTM, lithium-ion battery, machine learning, state of charge, state of health.

## NOMENCLATURE

| | |
|---|---|
| *BHO* | Bayesian Hyperparameter Optimization. |
| *BiGRU* | Bidirectional Gated Recurrent Unit. |
| *BiLSTM* | Bidirectional Long-Short Term Memory. |
| *BMS* | Battery Management System. |
| *DRNN* | Dynamic Recurrent Neural Network. |
| *DVA* | Differential Voltage Analysis. |
| *EV* | Electric Vehicle. |
| *FC* | Fully Connected. |
| *FLOPs* | FLoating-point OPerations. |
| *GRU* | Gated Recurrent Unit. |
| *HPPC* | Hybrid Pulse Power Characterization. |
| *ICA* | Increamental Capacity Analysis. |
| *LIBs* | Lithium-Ion Batteries. |
| *LS − SVM* | Least Square Support Vector Machine. |
| *LSTM* | Long-Short Term Memory. |
| *MAE* | Mean Absolute Error. |
| *NN* | Neural Network. |
| *NMC* | Nickel Manganese Cobalt. |
| *NSSR* | Nonlinear State Space Reconstruction. |
| *OCV* | Open Circuit Voltage. |
| *RMSE* | Root Mean Squared Error. |
| *SOC* | State of Charge. |
| *SOH* | State of Health. |
| *SOX* | State of Eveything. |
| *SWPSO* | Self-adaptive Weight Particle Swarm Optimization. |
| *UDDS* | Urban Dynamometer Driving Schedule. |
| *UPF* | Unscented Particle-Filter. |

The associate editor coordinating the review of this manuscript and approving it for publication was Wencong Su.

## I. INTRODUCTION

According to the updated 2030 framework of the European Union for climate and energy [1], a significant reduction in greenhouse gas emissions is targeted. The implementation of renewable energy sources and the transition towards electric mobility will contribute to achieving those environmental and energy goals [2]. Electrochemical batteries serve as an effective energy storage option for this transition [3], and the integration of a precise and efficient Battery Management System (BMS) can ensure their optimal functionality [4]. Typically, a state-of-the-art BMS should be capable of cell monitoring the voltage, current, and temperature while ensuring the safety and management of the cell [5]. Moreover, it should be capable of accurately estimating the State of Charge (SOC) [6] and the State of Health (SOH) [7] in Electric Vehicles (EV) [8], as these parameters are crucial for optimal operation, especially for Lithium-Ion-Batteries (LIBs) [9]. Inaccurate SOC estimation can result in overcharging of the battery [10], leading to a shortened battery lifespan, reduced energy efficiency, and potential safety concerns such as overheating, cell damage, or even hazardous situations [11]. Furthermore, battery degradation increases the internal resistance, and reduces its capacity and the overall performance of EVs over time [12]. Erroneous SOH estimations affect the battery lifespan, safety, and reliability [13].

State of Everything (SOX) estimation depended on intricate mathematical models rooted in electrochemical theories, necessitating in-depth knowledge, elaborate computations, and thorough calibration [14], [15]. Yet, these approaches often falter when facing real-world complexities, leading to imprecise results. Recently, Machine Learning (ML) emerged as a promising approach for SOX estimation [16], [17], employing data-driven algorithms to discern complex correlations between battery parameters and SOC accurately.

For this purpose, many methodologies have been developed for the joint SOC-SOH estimation [18]. Generally, many model-based methodologies have been developed for LIB [19], while lately, data-driven techniques have started emerging in this field, without a major breakthrough. Besides, a significant drawback of using these techniques is the uncertainty surrounding the model's hyperparameters, which can affect the precision of the predictions [16]. Consequently, in [20], the authors present a novel method for identifying the SOC and SOH of LIBs based on an improved Dynamic Recurrent Neural Network (DRNN) and Self-adaptive Weight Particle Swarm Optimization (SWPSO) algorithm. The DRNN is designed to capture the dynamic behaviour of the battery, while the SWPSO algorithm optimizes the network parameters to improve the accuracy of the estimation. Results indicate that this method surpasses other techniques like gradient descent-DRNN and back propagation-NN under various conditions.

In [21] the authors use the Nonlinear State Space Reconstruction (NSSR) approach to reconstruct the state space of the EV battery pack and Long-Short Term Memory (LSTM) to estimate its SOC and SOH. The proposed model excelled by achieving an RMSE of less than 2.5% for SOC estimation and 1.3% for SOH estimation at 25°C. Furthermore, in [22], the authors developed a hybrid Least Square Support Vector Machine (LS-SVM) and Unscented Particle-Filter (UPF) method for estimating the SOC and SOH of the LIBs in different time scales. The LS-SVM estimates the battery states, which are subsequently optimised by UPF. The experimental results show that the proposed method achieves high accuracy in estimating the SOC and SOH at 25°C with an RMSE of 2.1% at the 240 Cycle. In addition, in [23], the authors developed a novel method for estimating the SOC and SOH of LIBs using a nonlinear autoregressive with exogenous inputs Neural Network (NN). This method outperformed the simple multilayer perceptron in terms of accuracy and robustness.

The body of literature investigated so far, offers valuable insights, but there are still significant gaps: many of the developed models for the joint SOC-SOH estimations have not been evaluated with dynamic and complex datasets that simulate real-life applications. Furthermore, in most cases, authors do not evaluate the impact of varying temperatures on SOC estimation and battery degradation. Finally, many methods do not employ any algorithm for hyperparameter tuning, leading to an inefficient model.

This study proposes a new method that jointly estimates both the SOC and SOH of LIBs, tackling all the aforementioned gaps in literature. The proposed method incorporates the aging effects of the batteries by using the estimated SOH as an input to the model for SOC estimation.

The accuracy of the proposed method and its computational cost are evaluated and compared to other state-of-the-art models, such as: LSTM, GRU, and BiGRU. For the most promising solutions, an in-depth analysis is conducted on the window span of the created time series for the SOC estimation, and the voltage ranges, the input feature and the timestep analysis for the SOH estimation. A bayesian optimisation with a gaussian process algorithm is employed to set the model hyperparameters. Furthermore, a novel set of hyperparameters is proposed to maintain minimal network volume, expanding the hyperspace to include aspects such as the learning rate of the optimizer and the number of: RNN layers, units in each RNN layer, FC layers and neurons in each FC layer as well as the relevant activation functions. This expansion allows the proposed method to identify near-optimal hyperparameters without extensive manual network engineering. For a conclusive evaluation of the proposed framework's industrial applicability, the FLOPs are calculated, offering significant insights into the computational resources required for each predictive step of the algorithm. For the proposed framework, a new battery dataset was obtained, which contains measurements acquired over a wide range of temperature conditions and aging stages using extended dynamic driving cycles. This dataset is made available online and can be used by the scientific community to develop models and perform comparative testing.

The paper is structured as follows. Section II introduces the datasets used to train and test the model, and Section III evaluates and compares state-of-the-art models for SOC and SOH estimations. Section IV presents the development of the proposed joint SOC-SOH method and a discussion about the results of the model, and lastly, in Section V, there are the conclusions of the overall paper.

## II. DATASETS

### A. EXPERIMENTAL SETUP

In this work, the results of a measurement campaign performed in the battery laboratory of TU Berlin with the collaboration of the Politecnico di Milano University are presented. The schematic representation of the experimental setup is depicted in Figure 1.

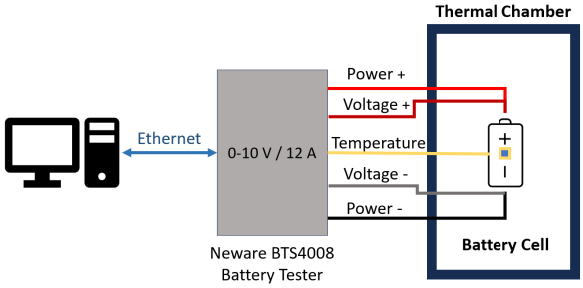


**FIGURE 1.** The schematic experimental setup.

Recorded data are related to a lithium NMC oxide LIB cell, and they can be split into two distinct phases: the SOC cycling and the degradation phase.

In the initial stage, a total of 8 LG18650HE4 battery cells with a capacity of 2.5 Ah were placed in a thermal chamber, specifically the Binder MK53. Due to a hardware malfunction, 2 cells were damaged during the cycling process and therefore the relevant data are not included in this analysis. For the charging and discharging of the battery cells, a Neware battery tester model BTS-4008 was used. Figure 2a shows the complete experimental setup, providing a comprehensive view of the overall arrangement. Meanwhile, Figure 2b illustrates the specific placement of the battery cells within the thermal chamber.

In the first phase, which involved the characterisation of SOC, the cells were subjected to static and dynamic cycling at six different ambient temperatures: −20°C, −10°C, 0°C, 10°C, 25°C, and 35°C, covering a wide range of temperatures scenarios. The dataset encompasses both static and dynamic stressing tests. The initial test involves the construction of the SOC-OCV curve by applying 1% SOC pulses, which helps establish the true relationship between SOC and the OCV. After, HPPC was performed at every 10% SOC interval to determine the charging and discharging internal resistance of the battery at each SOC level. Finally, for dynamic stress, there are four distinct driving cycles: the UDDS, the Highway Driving Schedule (US06), and the California Unified Cycle (LA92). Additionally, mixed cycles were created on purpose,

(a) The experimental setup at the battery laboratory at TU Berlin.

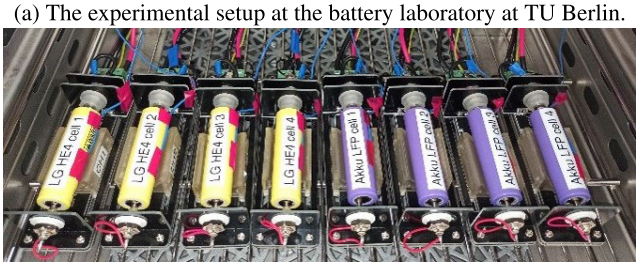


(b) Li-Ion battery cells: four NMC (yellow) and four LFP (blue).

**FIGURE 2.** Two aspects of the experimental setup.

by combining randomized segments from UDDS, US06, and LA92, named with increasing numbers from "Mixed1" to "Mixed6". Each driving cycle was performed at the six aforementioned ambient temperatures, and data were recorded at a sampling interval of 0.1 seconds. Figure 3 displays the complete cycling schedule, with the SOC Cycling cycle depicted in green blocks, the SOC Cycling test schedule in blue blocks, the SOH ageing cycling in orange blocks, the ageing schedule in grey, and the stress cycles in yellow. The stress cycles consist of Driving Cycles, HPPC tests, and SOC-OCV stress tests.

In the second phase, the battery cells were subject to the same driving cycles at a constant temperature of 35°C, aiming to simulate both driving and calendar ageing effects. To monitor the ageing process, a capacity test was conducted approximately every 20 to 30 cycles, while the impact of the ageing procedure can be observed in Figure 4. In this phase, data were recorded at a sampling interval of 1 second.

The final and complete open dataset, which was thus created covering various temperature ranges and ageing phases with dynamic driving cycles, is made available online [24]. It can be used by the scientific community and stakeholders for several purposes as any other model development and leading comparison tests.

### B. DATA PREPROCESS

Following data acquisition, a series of procedures were meticulously executed to clean the dataset and convert it into a form that can be easily implemented into the model. These preprocessing steps encompassed essential operations,

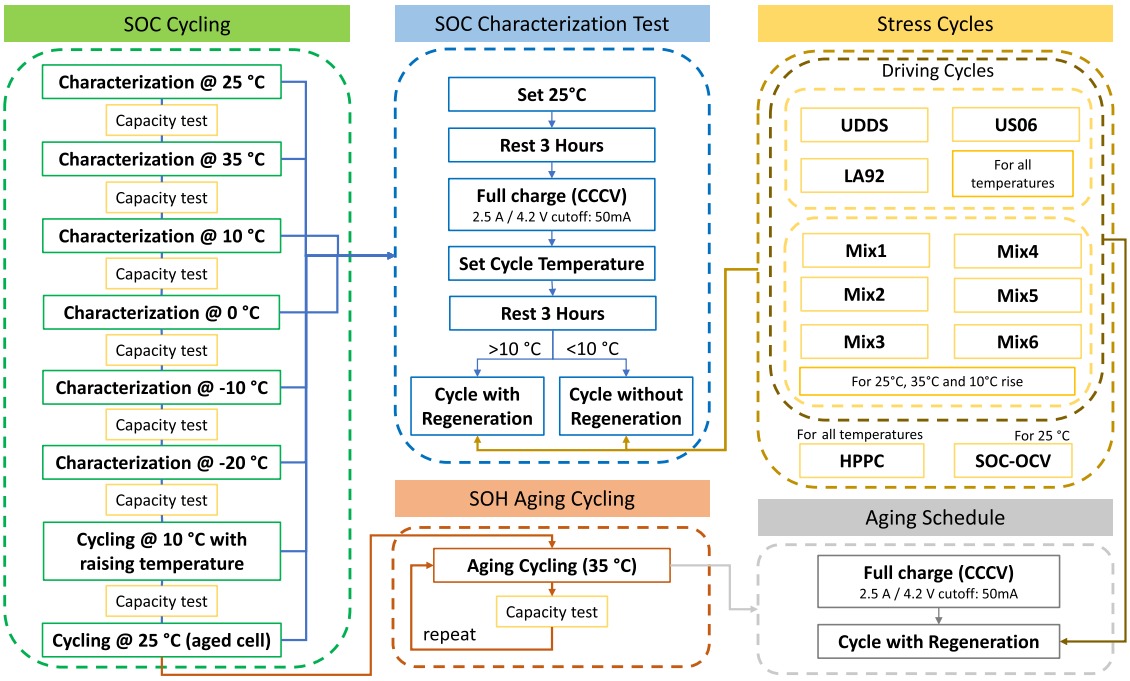


**FIGURE 3.** Experimental procedure for the creation of the dataset.

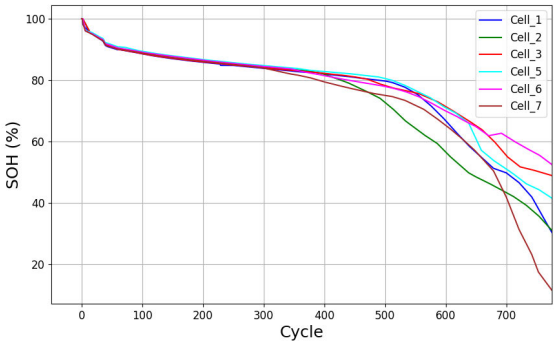


**FIGURE 4.** SOH trend of the analyzed NMC cells.

including the elimination of redundant data points, feeling missing data, and calculating SOC, by dividing the actual capacity with the actual capacity extracted in each cycle and SOH, by dividing the actual maximum capacity obtained by the capacity test with the initial maximum capacity. Furthermore, the data files underwent compression and meticulous organisation for enhanced manageability, where data from charging, discharging and driving cycles were separated. Subsequently, the dataset was expanded with ICA information derived from discharge and charge capacity differentiations with respect to the terminal voltage and DVA data obtained through terminal voltage differentiation with respect to the discharge and charge capacities. To prepare the ICA and DVA data for feature extraction, the Savitzky-Golay filter was thoughtfully applied to mitigate spikes and enhance their suitability for subsequent modelling processes.

Currently, data are divided into two main categories: the first relates to dynamic driving cycles for the SOC estimation, while the second category contains the data of the charging and discharging cycles for the SOH estimation. Additionally, to the latter category, supplementary details of the ICA and DVA curves were included to be used as input features for the SOH estimation.

## III. SoC AND SoH ESTIMATION

### A. METHODS

The main objective of this paper is to explore and compare different methods and models for improving the SOC and SOH estimation. In this section, there will be an analysis of two methods for the SOC estimation and one method for the SOH estimation which are depicted in Figure 5. Regarding SOC estimation, 'Method A' employs the terminal voltage, current, and surface temperature data of the driving cycles to predict SOC while in 'Method B', the real SOH data, which was calculated by the capacity tests as mentioned above, is added as an additional input whilst retaining the other parameters. Both methods were trained using driving cycles UDDS, US06, and Mixed 1 to 4. For the evaluation of the model, the LA92 and Mixed 5 and 6 cycles were utilized.

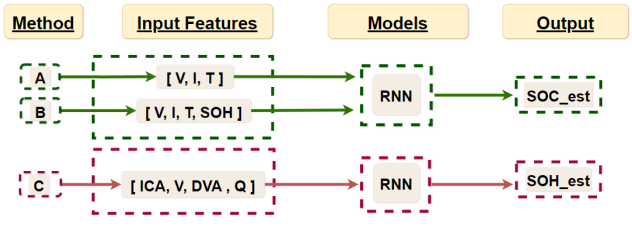


**FIGURE 5.** SOC and SOH estimation methods.

For both methods, the input consists of time-series data of the aforementioned features and is organized in matrices with length that is determined according to the time window value as it is presented in Figure 6. The model will make a single estimation for every time window, taking into consideration the past feature information.

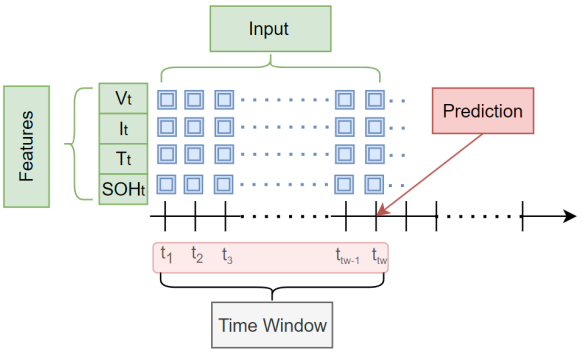


**FIGURE 6.** Time window of the time series created for the prediction of SOC in the 'Method B'.

Regarding the SOH, as depicted in Figure 5, 'Method C' utilises the terminal voltage, the capacity, the ICA, and the DVA as input features of the charging cycles to estimate the SOH. In this method, the data that will be used corresponds to partial charging, utilising part of the charging cycle to emulate the real-data availability. Additionally, the model was trained using the partial charging data from cells No. 1, 2, 3, 5, and 6. Cell No. 7, on the other hand, was utilized for the model's evaluation purposes.

For all the above methods, the authors consider four RNN models: LSTM, biLSTM, GRU, and biGRU, to compare their performance in estimating the SOC/SOH. For the RNN optimisation, the Bayesian Hyperparameter Optimization (BHO) is applied to search the optimal hyperparameters within specific parameter spaces. In this research, the parameters of the hyperspace can be found in Table 1 for the SOC and SOH models. This hyperspace is based on the previous work of the authors [25], exploring a broader range of parameters to enhance its overall accuracy. The proposed changes increase the number of additional RNN and FC layers from 2 to 4, increase the searching step of both layers from 4 to 8, incorporate the learning rate between the values [$10^{-3}$, $10^{-4}$ and $10^{-5}$] while searching for the activation function of the FC layers between the values of Leaky Rectified Linear Unit (leaky/ReLU), Gaussian Error Linear Unit (GELU), Swish, Scaled Exponential Linear Unit (SELU) and Linear.

**TABLE 1.** Hyperspace for the SOC and SOH models.

| Parameters | Hyperspace SOC | Hyperspace SOH |
|---|---|---|
| No. of additional RNN layers | 2-4 | |
| No. of additional Dense layers | 2-4 | |
| Max No. of RNN units | 64 | 15 |
| Max No. of Dense units | 64 | 15 |
| Searching step of RNN units | 8 | 1 |
| Searching step of Dense units | 8 | 1 |
| Learning rate | 1e-3, 1e-4, 1e-5 | |
| Dense activation function | leaky-relu, gelu, swish, selu, linear | |

### B. RECURRENT NEURAL NETWORKS

RNNs are artificial neural networks designed for processing sequential data, incorporating structures like LSTM, GRU, BiLSTM, and BiGRU. Their architectures create a form of memory that can capture past information, making them capable of predicting based on both the current input and the sequence of past inputs. This is achieved through loops within the network that pass information from one step of the sequence to the next. Compared to other networks, RNNs excel in tasks that require understanding temporal dynamics or sequential patterns, such as language translation, speech recognition, and time series prediction, due to their ability to handle variable-length sequences and their inherent capacity for capturing temporal dependencies.

#### 1) LSTMs AND GRUs

LSTM networks are a special kind of RNNs designed to overcome the limitations of traditional RNNs, particularly issues related to long-term dependencies. The architecture of an LSTM unit includes three gates: the input gate, the forget gate, and the output gate. These gates collectively decide what information should be passed on to the output, what should be retained in memory, and what should be forgotten. This mechanism allows LSTMs to preserve information over long periods, making them highly effective for tasks involving complex, sequential data like language modelling and time series analysis. The strength of LSTMs lies in their ability to capture long-term dependencies and process data sequences of variable lengths, which is a significant advantage over simpler neural network architectures.

GRUs are another type of RNNs similar to LSTMs but with a simplified structure. GRUs combine the forget and input gates into a single update gate and merge the cell state and hidden state, resulting in a more streamlined model that can be easier to train than LSTMs while achieving similar performance on certain tasks. The main differences between LSTMs and GRUs lie in their architecture and efficiency: GRUs are generally faster to train due to their simpler structure, but LSTMs may perform better on tasks that require modelling more complex dependencies. Both LSTMs and GRUs are preferred over simple RNNs because they significantly reduce the vanishing gradient problem, allowing for better learning of long-range dependencies within the data.

#### 2) BiLSTMs AND BiGRUs

BiLSTMs extend the concept of LSTMs by processing the data in both forward and backward directions. This dual processing enables the network to have both past and future context at any point in the sequence, providing a richer understanding of the sequence's context. The architecture of a BiLSTM consists of two LSTMs layers that are applied

in parallel: one processes the sequence from start to end, while the other processes it from end to start. The outputs of both layers are then combined. This bidirectional approach is particularly beneficial for tasks where the context from both directions is crucial, such as in natural language processing and speech recognition.

BiGRUs apply the same bidirectional concept to the GRU architecture. Similar to BiLSTMs, BiGRUs process data both forward and backward, combining the strengths of GRUs with the ability to capture information from both past and future contexts. The main difference between BiLSTMs and BiGRUs, like with their unidirectional counterparts, lies in their internal structure and efficiency. BiGRUs offer a simpler, more efficient alternative to BiLSTMs, potentially reducing training time without significantly sacrificing performance. The choice between BiLSTM and BiGRU typically depends on the specific requirements of the task, such as the complexity of the temporal dependencies and the computational resources available. Both bidirectional models represent a significant advancement over their simple LSTM and GRU counterparts by providing a more comprehensive understanding of sequential data.

### C. BAYESIAN HYPERPARAMETER OPTIMIZATION

One of the biggest challenges in data-driven methods is the optimisation of the model's hyperparameters. For the identification of the optimal ones, exhaustive methods such as the Grid Search (GS), the Manual Search (MS) and the Random Search can be applied. The GS and the MS are computationally expensive methods, especially when there is a large number of hyperparameters and a wide range of values to search through. Additionally, the RS method is a purely stochastic procedure, which can lead to an inefficient search for optimal values. On the other hand, probabilistic methods, such as the Bayesian optimisation algorithm, combine the advantages of the methods mentioned above while providing near-optimal values with fewer trials as it considers the previous evaluations [26].

The BHO is an iterative optimisation method designed to find the global optimum of a complicated function efficiently. It constructs a probabilistic surrogate model, usually a Gaussian process, to approximate the function's behaviour and uncertainty. This surrogate model guides the optimisation process by balancing exploration (seeking unexplored regions of the parameter space) and exploitation (focusing on areas likely to yield better results). At each iteration, BHO selects the next set of parameters to evaluate based on an acquisition function that quantifies this trade-off. After evaluating the chosen parameters, the surrogate model is updated, and the process continues until convergence to the optimal solution or a predefined stopping criterion is met [27]. In this paper, the authors will examine two hyperparameter spaces, one for the SOC model and one for the SOH model, utilising identical parameters for optimisation but with different ranges, as illustrated in Table 1.

### D. METRICS

In this subsection, there will be an analytical presentation of the results obtained by implementing the methods presented above, utilising the battery dataset of section II. Initially, there will be an analysis of the two different 'Methods A' and 'B' for the SOC prediction and a comparison between them. Afterwards, the performance of 'Method C' for predicting the SOH will be presented.

For evaluating the model's performance, three metrics were applied: The RMSE, the MAE, and the FLOPs. The first two metrics are given by:

$$RMSE = \sqrt{\frac{1}{n}\sum_{i=1}^{n}(y-\hat{y})^2} \tag{1}$$

$$MAE = \frac{1}{n}\sum_{j=1}^{n}|y-\hat{y}| \tag{2}$$

where $y$ is the real value of the SOC or SOH while the $\hat{y}$ is the predicted value generated by the model.

The last metric refers to the number of floating-point arithmetic operations (additions and multiplications) performed during a model's forward and backward passes, and it is used to measure the computational complexity of the model using the Keras library [28].

### E. SOC PREDICTION MODEL

For the SOC prediction, as mentioned before, two different methods (A and B) were developed, as Figure 5 depicts. As a training dataset, data from cell No. 1 have been used encompassing both the 'SOC Cycling' and the 'SOH Aging Cycling' up to a SOH value of 70%, were utilized. This was chosen to compare across the entire first life of the battery. 'Method A' uses voltage, current and surface temperature as input data, while 'Method B' employs one extra feature, which is the SOH of the battery. For this analysis, the SOH information that was used is the true value determined by dividing the maximum capacity available in the current cycle by the initial maximum capacity available.

To conduct a thorough comparison of the two methods, both layer and time window analyses were utilized to determine the model configuration that produced the minimum error. In both scenarios, the time series generated was set to 40s for the layer analysis according to the finding in [25] for similar datasets. Subsequently, time window analyses for 20, 30, 40, and 80 seconds were implemented for the layer that exhibited superior performance. For all aforementioned analyses, the BHO was employed according to the hyperspace in Table 1.

#### 1) METHOD A

Starting with 'Method A', for the layer analysis setting a 40s time window as previously stated, the LSTM model provides the lowest error compared with the rest of the models, with an MAE of 1.69% and an RMSE of 2.59%. The outcomes of this first analysis are reported in Table 2. After the time window

analysis, the 60s were shown the best predictive capability compared to the other time window values with an MAE of 1.66% and an RMSE of 2.51%. The results of the second analysis are presented in Table 3.

#### 2) METHOD B

For the layer analysis, the same time window of the 40s was used, revealing the predictive capability of the BiLSTM model achieving the most accurate results, with an MAE of 1.32% and an RMSE of 2.51%. For the time window analysis, the 80s yielded the best results, considering the RMSE value, with an MAE of 1.42% and an RMSE of 2.31%. Table 2 and Table 3 present the overall results of the layer and time window analysis for 'Method B'.

**TABLE 2. RMSE, MAE of the predicted SOC, and FLOPs for the four layers performance for 'Method A' and 'Method B' with 40s time-window span.**

| | Layers | GRU | BiGRU | LSTM | BiLSTM |
|---|---|---|---|---|---|
| Arch. A | MAE (%) | 1.83 | 1.68 | 1.69 | 1.99 |
| | RMSE (%) | 2.78 | 2.69 | 2.59 | 2.77 |
| | FLOPs (k) | 1230.1 | 265 | 141.9 | 160.4 |
| Arch. B | MAE (%) | 2.05 | 2.26 | 1.59 | 1.32 |
| | RMSE (%) | 3.04 | 3.15 | 3.05 | 2.51 |
| | FLOPs (k) | 730.2 | 1417.3 | 4677.8 | 8291.2 |

**TABLE 3. RMSE, MAE of the predicted SOC, and FLOPs for the time window analysis using the best results of the layer analysis, for the 'Method A' the LSTM layer and for the 'Method B' the BiLSTM layer.**

| | Time Window | 20s | 40s | 60s | 80s |
|---|---|---|---|---|---|
| Method A (LSTM) | MAE (%) | 1.85 | 1.69 | 1.66 | 2.36 |
| | RMSE (%) | 2.60 | 2.59 | 2.51 | 3.44 |
| | FLOPs (k) | 141.9 | 141.9 | 765.5 | 467.8 |
| Arch. B (BiLSTM) | MAE (%) | 2.41 | 1.32 | 1.66 | 1.42 |
| | RMSE (%) | 3.45 | 2.51 | 2.62 | 2.31 |
| | FLOPs (k) | 813.4 | 829.1 | 813.4 | 1492.3 |

#### 3) METHOD A AND B COMPARISON

It's evident that for the case of 'Method A' the LSTM model yields better results while for 'Method B' the BiLSTM model achieves the smallest error margins across all scenarios. While Method A performs best with a 60-second window and Method B with an 80-second window, there's an interesting observation. A 40-second interval leads to lower MAE for 'Method B', suggesting higher overall accuracy in capturing trends. However, for accurate SOC estimation, minimizing large errors is critical, since RMSE penalizes larger errors more heavily, and smaller RMSE values in 'Method B' at the 80-second window indicate its superiority in this specific task. Overall, 'Method B' demonstrates a 16% decrease in MAE and an 11% reduction in RMSE when contrasted with 'Method A'.

Considering the dynamic degradation of the battery throughout the first life of the battery cell, the BiLSTM models with an 80-second time window from both methods were evaluated at every 40 to 50 cycles, and during each cycle of the mixed 6 and 7 and LA92 cycles, until the SOH reached 70%. The results of the average MAE of the methods are presented in Figure 7. As was expected, the information on SOH plays a vital role in accurately predicting SOC, specifically when the battery degradation moves further with a substantial reduction in the estimation error.

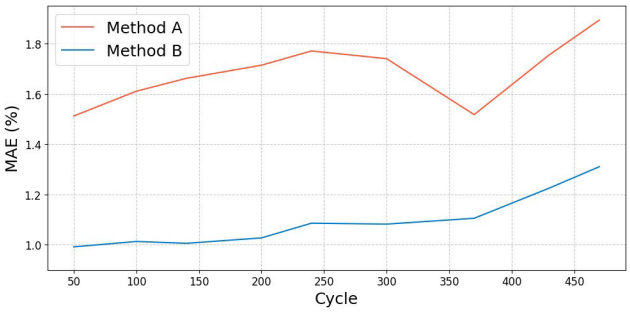


**FIGURE 7. Average MAE of SOC estimation for the dynamic ageing phase between the two methods.**

### F. SOH PREDICTION MODEL

After analyzing the SOC estimation, subsequently, the results for 'Method C' in the SOH estimation are presented. Data from the 'SOH Ageing Cycling' phase, based on charging cycles, are utilised for the BHO procedure of the models. Furthermore, various factors such as voltage range, sampling time, and input features were meticulously examined to identify the model yielding the most precise results. Concerning the voltage range, partial charging data were utilised to simulate a real-world scenario where an EV is connected to the charger with more than 0% SOC level and departs the station with less than a 100% SOC level. In terms of sampling time, a comparative analysis was conducted between 1 second and 10 seconds. Lastly, a combination of the four parameters, the voltage, the capacity, the ICA and the DVA were selected as input features for exhaustive testing and evaluation. In Table 4 and Table 5 is presented the ranges of the parameters and the overall comparative analysis for all the models of Method C, respectively, while in Table 6 the top three models that yielded the best results are depicted.

**TABLE 4. Parameters of method C.**

| Parameters | Values |
|---|---|
| Model | GRU, LSTM, BiGRU, BiLSTM |
| Voltage ranges (V) | 3.6-4.0, 3.6-3.9, 3.7-4.0 |
| Sampling Time (s) | 1 or 10 |
| Input features | ICA, ICA V, ICA V DVA, ICA V DVA Q |

Based on the findings presented in Table 6, the top three models exhibited comparable predictive accuracy, each with an MAE of approximately 0.3%. Model No. 3 was identified as the most suitable choice, owing to its requirement for a narrower voltage range for estimation, the minimal number of input features needed (solely the ICA), and the reduced computational demand in terms of FLOPs. This efficiency makes it particularly well-suited for electronic applications,

**TABLE 5.** Comparative analysis for all models of method C in estimating SOH.

| Voltage Range | Sampling Time | Input Features | MAE (%) | | | | RMSE (%) | | | | FLOPS | | | |
|---|---|---|---|---|---|---|---|---|---|---|---|---|---|---|
| | | | LSTM | GRU | BiGRU | BiLSTM | LSTM | GRU | BiGRU | BiLSTM | LSTM | GRU | BiGRU | BiLSTM |
| 3.6 to 3.9 | 10s | ICA | 0.61 | 1.14 | 0.66 | 0.67 | 0.78 | 1.29 | 0.95 | 1.02 | 36608 | 2176 | 9152 | 69312 |
| | | ICA, V | 1.03 | 0.91 | 0.59 | 0.65 | 1.07 | 1.02 | 0.85 | 0.71 | 91264 | 2176 | 60544 | 65408 |
| | | ICA, DVA, V | 085 | 0.93 | 0.86 | 0.52 | 0.92 | 0.97 | 0.99 | 0.72 | 7040 | 2688 | 36736 | 60544 |
| | | ICA, DVA, V, Q | 0.66 | 0.88 | 0.81 | 0.55 | 0.89 | 1.22 | 0.95 | 0.75 | 31744 | 61696 | 5120 | 60544 |
| | 1s | ICA | 0.72 | 1.09 | 0.5 | 0.3 | 1.05 | 1.33 | 0.69 | 0.42 | 32128 | 4846 | 65408 | 1024 |
| | | ICA, V | 0.73 | 1.09 | 0.77 | 0.48 | 0.98 | 1.54 | 0.91 | 0.63 | 31744 | 91264 | 4096 | 3584 |
| | | ICA, DVA, V | 0.71 | 1.27 | 0.81 | 0.31 | 1.05 | 1.60 | 0.93 | 0.46 | 3840 | 31744 | 38528 | 8960 |
| | | ICA, DVA, V, Q | 0.86 | 0.88 | 0.43 | 0.77 | 1.13 | 1.2 | 0.58 | 0.79 | 9728 | 61696 | 6784 | 11008 |
| 3.7 to 4.0 | 10s | ICA | 0.81 | 0.49 | 1.36 | 0.97 | 1.16 | 0.75 | 1.46 | 1.12 | 7040 | 6848 | 4096 | 60928 |
| | | ICA, V | 0.64 | 0.64 | 0.91 | 0.88 | 0.90 | 0.85 | 0.91 | 1.05 | 3008 | 31744 | 11008 | 7168 |
| | | ICA, DVA, V | 0.58 | 1.05 | 1.03 | 0.74 | 0.80 | 1.24 | 1.29 | 1.09 | 4864 | 9280 | 49728 | 9216 |
| | | ICA, DVA, V, Q | 0.64 | 0.91 | 0.59 | 0.82 | 0.70 | 1.01 | 0.81 | 0.91 | 38336 | 33600 | 38528 | 60544 |
| | 10s | ICA | 0.95 | 0.88 | 0.88 | 1.27 | 1.27 | 0.99 | 1.03 | 1.55 | 7424 | 91264 | 6784 | 6784 |
| | | ICA, V | 1.25 | 0.76 | 1.15 | 1.13 | 1.59 | 0.98 | 1.36 | 1.30 | 9728 | 9280 | 120064 | 8960 |
| | | ICA, DVA, V | 1.12 | 0.50 | 0.83 | 0.93 | 1.36 | 0.75 | 1.09 | 1.24 | 25984 | 64384 | 4096 | 7168 |
| | | ICA, DVA, V, Q | 0.64 | 0.83 | 0.41 | 0.63 | 0.82 | 1.01 | 0.55 | 0.73 | 5248 | 4864 | 20992 | 90304 |
| 3.6 to 4.0 | 10s | ICA | 1.07 | 0.59 | 0.42 | 0.41 | 1.27 | 0.75 | 0.51 | 0.63 | 12544 | 42752 | 10240 | 5824 |
| | | ICA, V | 0.76 | 0.70 | 0.52 | 0.54 | 1.02 | 0.92 | 0.67 | 0.69 | 6976 | 6976 | 5824 | 11584 |
| | | ICA, DVA, V | 0.55 | 0.61 | 0.30 | 0.35 | 0.88 | 0.88 | 0.40 | 0.40 | 11328 | 13568 | 11968 | 28224 |
| | | ICA, DVA, V, Q | 0.75 | 0.53 | 0.36 | 0.29 | 1.06 | 0.73 | 0.46 | 0.35 | 2880 | 7808 | 10240 | 43520 |
| | 1s | ICA | 0.60 | 0.52 | 0.67 | 0.38 | 0.71 | 0.69 | 0.74 | 0.43 | 2880 | 42752 | 66048 | 13568 |
| | | ICA, V | 0.47 | 0.83 | 0.48 | 0.58 | 0.68 | 0.99 | 0.56 | 0.65 | 29184 | 13568 | 66048 | 28672 |
| | | ICA, DVA, V | 0.49 | 0.42 | 0.54 | 0.93 | 0.70 | 0.61 | 0.65 | 1.34 | 34048 | 29184 | 44800 | 5440 |
| | | ICA, DVA, V, Q | 0.37 | 0.56 | 0.31 | 0.32 | 0.53 | 0.62 | 0.39 | 0.50 | 34048 | 24832 | 20544 | 14656 |

**TABLE 6.** Top three performances of Method C in estimating SOH.

| Parameters | Values | | |
|---|---|---|---|
| No. | 1 | 2 | 3 |
| Model | BiLSTM | BiGRU | BiLSTM |
| Voltage ranges (V) | 3.6-4.0 | 3.6-4.0 | 3.6-3.9 |
| Sampling Time (s) | 10 | 10 | 1 |
| Input features | ICA V DVA Q | ICA V DVA | ICA |
| MAE (%) | 0.29 | 0.30 | 0.30 |
| RMSE (%) | 0.35 | 0.40 | 0.42 |
| FLOPs | 43520 | 11968 | 1024 |

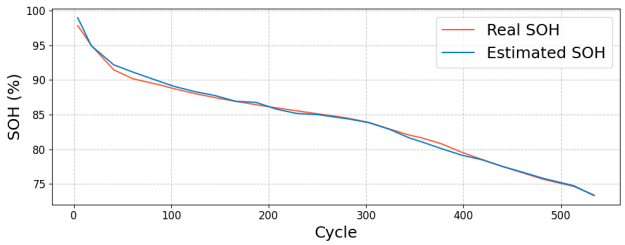


**FIGURE 8.** Real SOH vs Estimated SOH of the BiLSTM model with ICA as input feature and partial charging from 3.6 to 3.9 V and 1s sampling time.

including the BMS of EVs. In Figure 8, a comparison is illustrated between the actual SOH values and the SOH values estimated using model No. 3.

## IV. PROPOSED METHOD FOR THE JOINT SOC-SOH FRAMEWORK

### A. METHOD

Finally, the proposed method, as described in Figure 9 combines 'Method B' and 'C' for the joint estimation of the SOC and SOH. In this solution, firstly, the 'Method C'-based model, with the BiLSTM as RNN layer, is utilised to

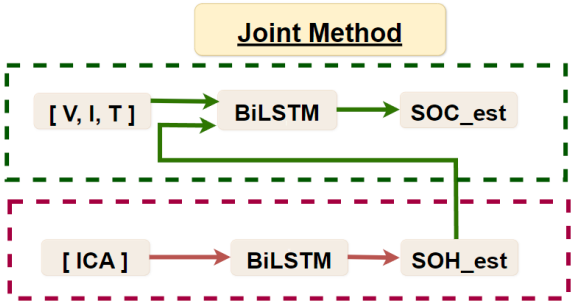


**FIGURE 9.** Proposed method for the joint SOC-SOH estimation consisting of 'Method B'-based BiLSTM model for the SOC estimation and an 'Method C'-based BiLSTM model for the SOH estimation.

estimate SOH values based on the partial charge cycles of the cell, imitating the charging procedure in an EV charging station, and then this information, along with terminal voltage, current, and surface temperature data of the driving cycle is fed into the 'Method B'-based model, again with BiLSTM as RNN layer, to estimate the SOC. In summary, the model comprises two distinct methods (B and C), each separately trained and tuned using BHO with a similar hyperspace creating a BiLSTM SOC model and a BiLSTM SOH model. This approach allows us to achieve satisfactory results without imposing excessive computational demands or memory requirements.

The model's hyperparameters were optimised using the BHO and the overall characteristics of the two models that compose the proposed method are presented in Table 7. To make the proposed method more relevant to industrial applications, the training dataset was constructed using data from cells No. 1, 2, 3, 5, and 6 for both models. Conversely, data from cell No. 7 was designated as the testing dataset.

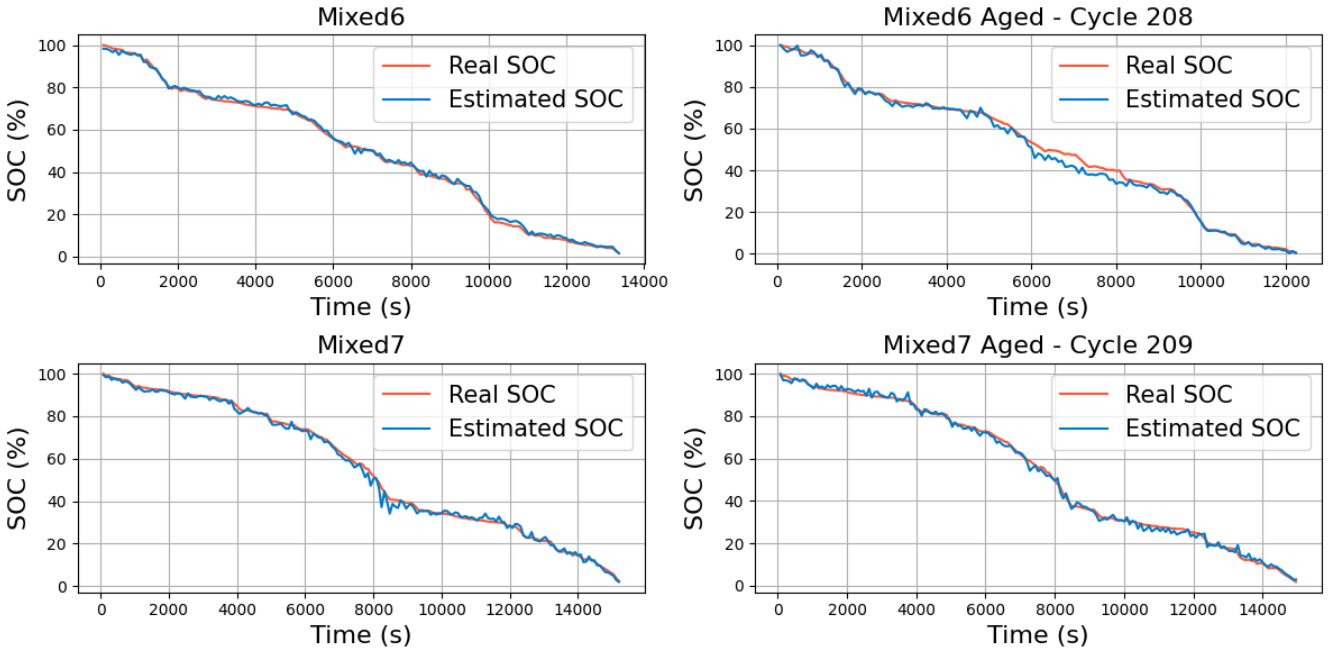


**FIGURE 10.** Real SOC vs Estimated SOC of the proposed method.

**TABLE 7.** Selected parameters of proposed method.

| Parameters | Characteristics | |
|---|---|---|
| Method | Method C | Method B |
| Model | BiLSTM | BiLSTM |
| Input features | ICA | V, I, T, SOH |
| Output feature | $SOH_{est}$ | $SOC_{est}$ |
| Sampling Time (sec) | 1 | 1 |
| Time Window (sec) | 910s | 80s |
| Voltage ranges (V) | 3.6-3.9 | - |

**TABLE 8.** SOC error compared to different SOH Data.

| Errors | Continuous Update | Step Update | Extrapolation Update | No SOH Data |
|---|---|---|---|---|
| MAE (%) | 1.54 | 1.71 | **1.52** | 1.98 |
| RMSE (%) | 2.57 | 3.07 | **2.50** | 3.21 |

By following this approach, the training phase involved data from five cells, while the model evaluation utilized data from an unseen cell. The dataset used encompassed both the 'SOC Cycling' and the 'SOH Aging Cycling' up to an SOH value of 70%. The specific training and testing cycles corresponded to those outlined in subsection III-A.

After the initial model training and throughout the whole first life of the battery, the ICA information of the partial charging cycles is inserted into the BiLSTM model for the SOH prediction, as demonstrated with Method C. Afterwards, the estimated SOH information is fed with the terminal voltage, current, and surface temperature measurements into the next BiLSTM model for estimating the SOC, likewise in Method B. According to the aforementioned analysis, the BiLSTM models were selected due to the best accuracy yielded for both methods. The general framework of this method is presented in Figure 11.

### B. RESULTS OF PROPOSED METHOD

For the proposed framework, the SOH data was estimated at the start of each cycle before the driving cycle. This mirrors a realistic situation where the EV is charged before embarking on its journey. Here, the SOH model could be integrated into either the EV's BMS or within the charging station, where it can send information to the EV's BMS. The results of the prediction of the SOC are presented in Figure 10, while the errors, the proposed method achieves MAE and RMSE of 1.52% and 2.5%, respectively, presented in Table 8.

Additionally, in scenarios where the SOH model resides in an EV charging station that is used only occasionally for charging, two distinct cases were analyzed. In the first case, the SOH data is updated during the use of this specific charging station and will only be refreshed upon the next usage of the same station, consequently called 'Step Update'. In the second case, following the update of the SOH data, a linear extrapolation is employed on the data following a switch to a different charging station, based on the variance observed between the two successive SOH updates from the EV charging station with the SOH model. The latter case is called 'Extrapolation Update'.

For the 1st case, the proposed model achieves MAE and RMSE 1.71% and 3.07%, respectively. For the 2nd case, the model achieves an MAE of 1.52% and an RMSE of 2.50%. Finally, for better comparison and evaluation of the proposed method, the predictive capability of the 'Method A'

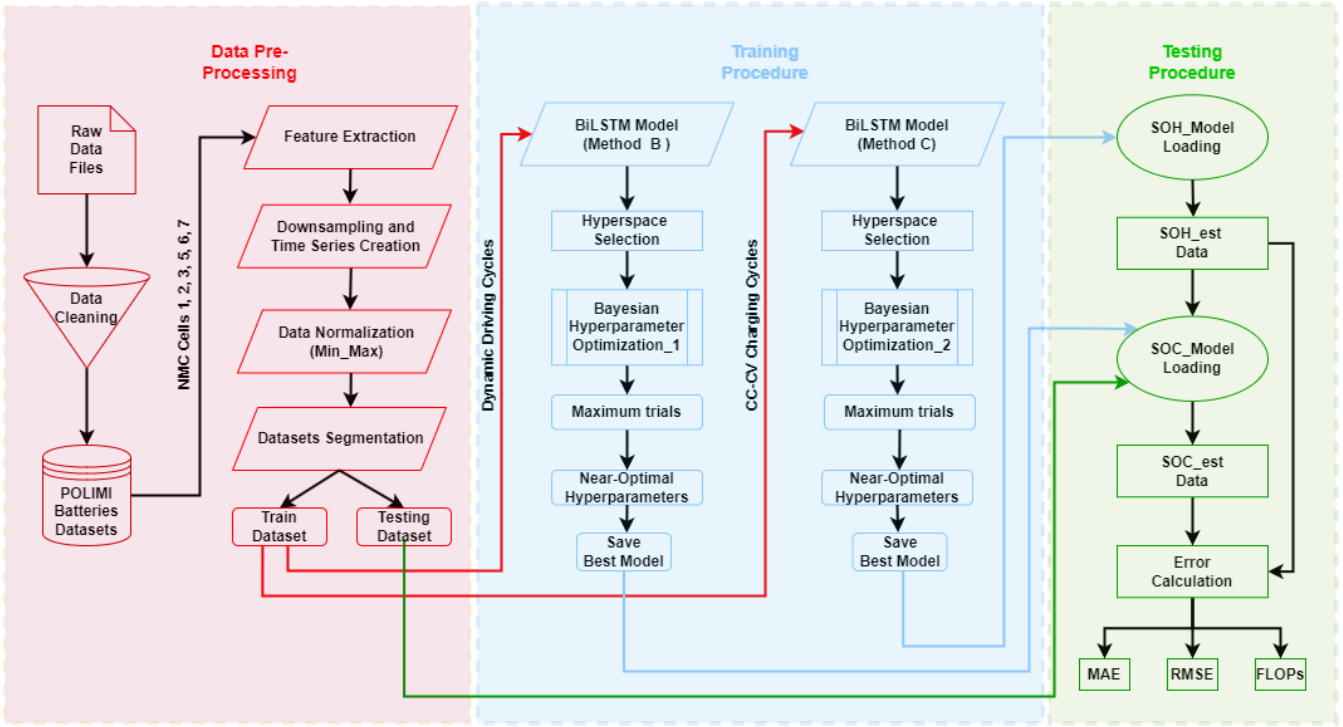


**FIGURE 11.** The total procedure for the joint SOC-SOH estimation model.

was tested. As was expected, the error, in this case, is greater with an MAE and an RMSE of 1.98% and 3.21%, respectively. In Table 8, there is a presentation of the above errors.

## V. CONCLUSION

The proposed framework introduces a new joint SOC-SOH estimation model innovatively designed to account for the ageing effects on lithium-ion batteries by integrating the SOH into the model inputs, enhancing the SOC estimations. The analysis demonstrated improved predictive accuracy when the SOH value was incorporated.

This study also introduces near-optimal hyperparameters for a more efficient streamlined network structure, expanding the exploration of hyperparameter space, including: optimizer rate, RNN layers, Fully Connected layers, and activation functions. An evaluation of the model's accuracy and computational expenditure was undertaken, positioning it against prevailing cutting-edge models. For the most promising configurations, a detailed analysis was executed, focusing on the time series' window span. The aforementioned analysis revealed the BiLSTM as the most appropriate predictive model for both SOC and SOH estimation. The proposed framework achieved an average MAE of 0.3% and an RMSE of 0.42% estimating the SOH and an average MAE of 1.42% and an RMSE of 2.31% estimating the SOC throughout the first life of the battery.

Future work should focus on integrating this framework into a BMS microcontroller, examining neural network compression for microcontroller suitability, and employing transfer learning techniques to evaluate the model's accuracy in new datasets and battery types. Finally, upscaling the model and testing it on battery modules/packs, rather than single cells, is advised to further validate the method.

## ACKNOWLEDGMENT

This manuscript reflects only the authors' views and opinions, neither the European Union nor the European Commission can be considered responsible for them. The authors would like to extend their sincere gratitude to Lars Krüger, Dominic Kupfer, and Mano Björn Schmit of the Technische Universität Berlin for their invaluable assistance, and technical support throughout the experimental process.

## REFERENCES

[1] E. Commission. (2030). *2030 Climate & Energy Framework*. [Online]. Available: https://climate.ec.europa.eu/eu-action/climate-strategies-targets/2030-climate-energy-framework_en

[2] D. B. Richardson, "Electric vehicles and the electric grid: A review of modeling approaches, impacts, and renewable energy integration," *Renew. Sustain. Energy Rev.*, vol. 19, pp. 247–254, Mar. 2013.

[3] R. Xiong, S. M. Sharkh, H. Li, H. Bai, W. Shen, P. Bai, and X. Zhou, "IEEE access special section editorial: Advanced energy storage technologies and their applications," *IEEE Access*, vol. 8, pp. 218685–218693, 2020.

[4] Y. Yang, S. Bremner, C. Menictas, and M. Kay, "Modelling and optimal energy management for battery energy storage systems in renewable energy systems: A review," *Renew. Sustain. Energy Rev.*, vol. 167, Oct. 2022, Art. no. 112671.

[5] M. Chen, G. Ma, W. Liu, N. Zeng, and X. Luo, "An overview of data-driven battery health estimation technology for battery management system," *Neurocomputing*, vol. 532, pp. 152–169, May 2023.

[6] M. Zhu, K. Qian, and X. Liu, "A three-time-scale dual extended Kalman filtering for parameter and state estimation of Li-ion battery," *Proc. Inst. Mech. Eng., D, J. Automobile Eng.*, vol. 238, no. 6, pp. 1352–1367, May 2024.
[7] J. Liu and X. Liu, "An improved method of state of health prediction for lithium batteries considering different temperature," *J. Energy Storage*, vol. 63, Jul. 2023, Art. no. 107028.
[8] H. Rahimi-Eichi, U. Ojha, F. Baronti, and M.-Y. Chow, "Battery management system: An overview of its application in the smart grid and electric vehicles," *IEEE Ind. Electron. Mag.*, vol. 7, no. 2, pp. 4–16, Jun. 2013.
[9] P. Dini, A. Colicelli, and S. Saponara, "Review on modeling and SOC/SOH estimation of batteries for automotive applications," *Batteries*, vol. 10, no. 1, p. 34, Jan. 2024.
[10] F. Mohammadi, "Lithium-ion battery State-of-Charge estimation based on an improved Coulomb-counting algorithm and uncertainty evaluation," *J. Energy Storage*, vol. 48, Apr. 2022, Art. no. 104061.
[11] Q. Wang, M. Ye, M. Wei, G. Lian, and C. Wu, "Co-estimation of state of charge and capacity for lithium-ion battery based on recurrent neural network and support vector machine," *Energy Rep.*, vol. 7, pp. 7323–7332, Nov. 2021.
[12] X. Han, L. Lu, Y. Zheng, X. Feng, Z. Li, J. Li, and M. Ouyang, "A review on the key issues of the lithium ion battery degradation among the whole life cycle," *eTransportation*, vol. 1, Aug. 2019, Art. no. 100005.
[13] J. Zhu, M. S. Dewi Darma, M. Knapp, D. R. Sørensen, M. Heere, Q. Fang, X. Wang, H. Dai, L. Mereacre, A. Senyshyn, X. Wei, and H. Ehrenberg, "Investigation of lithium-ion battery degradation mechanisms by combining differential voltage analysis and alternating current impedance," *J. Power Sources*, vol. 448, Feb. 2020, Art. no. 227575.
[14] J. Hou, T. Li, F. Zhou, D. Zhao, Y. Zhong, L. Yao, and L. Zeng, "A review of critical state joint estimation methods of lithium-ion batteries in electric vehicles," *World Electr. Vehicle J.*, vol. 13, no. 9, p. 159, Aug. 2022.
[15] D. N. T. How, M. A. Hannan, M. S. H. Lipu, and P. J. Ker, "State of charge estimation for lithium-ion batteries using model-based and data-driven methods: A review," *IEEE Access*, vol. 7, pp. 136116–136136, 2019.
[16] P. Eleftheriadis, S. Giazitzis, S. Leva, and E. Ogliari, "Data-driven methods for the state of charge estimation of lithium-ion batteries: An overview," *Forecasting*, vol. 5, no. 3, pp. 576–599, Sep. 2023. [Online]. Available: https://www.mdpi.com/2571-9394/5/3/32
[17] P. Eleftheriadis, S. Giazitzis, C. Ozmalatyalilar, S. Leva, and R. Zich, "An overview of data-driven methods for the state of health estimation," in *Proc. IEEE Int. Conf. Environ. Electr. Eng. IEEE Ind. Commercial Power Syst. Eur. (EEEIC/I&CPS Eur.)*, Jun. 2023, pp. 1–6.
[18] F. Liu, D. Yu, C. Shao, X. Liu, and W. Su, "A review of multi-state joint estimation for lithium-ion battery: Research status and suggestions," *J. Energy Storage*, vol. 73, Dec. 2023, Art. no. 109071.
[19] K. Qian and X. Liu, "Hybrid optimization strategy for lithium-ion battery's state of charge/health using joint of dual Kalman filter and modified sine-cosine algorithm," *J. Energy Storage*, vol. 44, Dec. 2021, Art. no. 103319.
[20] Y. Che, Y. Liu, Z. Cheng, and J. Zhang, "SOC and SOH identification method of Li-ion battery based on SWPSO-DRNN," *IEEE J. Emerg. Sel. Topics Power Electron.*, vol. 9, no. 4, pp. 4050–4061, Aug. 2021.
[21] P. Hu, W. F. Tang, C. H. Li, S.-L. Mak, C. Y. Li, and C. C. Lee, "Joint state of charge (SOC) and state of health (SOH) estimation for lithium-ion batteries packs of electric vehicles based on NSSR-LSTM neural network," *Energies*, vol. 16, no. 14, p. 5313, Jul. 2023.
[22] Y. Song, D. Liu, H. Liao, and Y. Peng, "A hybrid statistical data-driven method for on-line joint state estimation of lithium-ion batteries," *Appl. Energy*, vol. 261, Mar. 2020, Art. no. 114408.
[23] H. Chaoui and C. C. Ibe-Ekeocha, "State of charge and state of health estimation for lithium batteries using recurrent neural networks," *IEEE Trans. Veh. Technol.*, vol. 66, no. 10, pp. 8773–8783, Oct. 2017.
[24] Eleftheriadis. (2024). *PoliMi-TUB Dataset LG 18650HE4 Li-Ion Battery*. [Online]. Available: https://data.mendeley.com/datasets/6hyhsjbwkb/1
[25] P. Eleftheriadis, S. Leva, and E. Ogliari, "Bayesian hyperparameter optimization of stacked bidirectional long short-term memory neural network for the state of charge estimation," *Sustain. Energy, Grids Netw.*, vol. 36, Dec. 2023, Art. no. 101160.
[26] L. Yang and A. Shami, "On hyperparameter optimization of machine learning algorithms: Theory and practice," *Neurocomputing*, vol. 415, pp. 295–316, Nov. 2020. [Online]. Available: https://www.sciencedirect.com/science/article/pii/S0925231220311693
[27] B. Shahriari, K. Swersky, Z. Wang, R. P. Adams, and N. de Freitas, "Taking the human out of the loop: A review of Bayesian optimization," *Proc. IEEE*, vol. 104, no. 1, pp. 148–175, Jan. 2016.
[28] Keras. (2020). *Keras-FLOPs*. Accessed: Jun. 10, 2023. [Online]. Available: https://pypi.org/project/keras-flops/

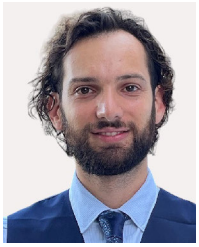

**PANAGIOTIS ELEFTHERIADIS** (Student Member, IEEE) received the Dipl.Eng. degree from the Aristotle University of Thessaloniki, in 2017, and the Ph.D. degree in electrical engineering from Politecnico di Milano, Italy, in May 2024. His research interests include AI, battery modeling, renewable energy sources, and power systems.

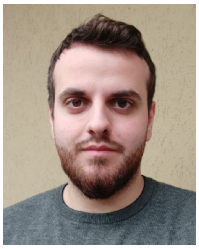

**SPYRIDON GIAZITZIS** received the Dipl.Eng. degree from the Aristotle University of Thessaloniki, in 2023. He is currently pursuing the Ph.D. degree. His research interests include AI, TinyML, batteries, and renewable energy sources.

**JULIA KOWAL** (Member, IEEE) is currently a Professor of electrical energy storage technology with the Institute for Energy and Automation Technology, TU Berlin. Her research interests include testing, characterisation, ageing, modelling, diagnostics, and lifetime prediction of different battery technologies.

**SONIA LEVA** (Senior Member, IEEE) received the Ph.D. degree in electrical engineering from Politecnico di Milano, Italy, in 2001. She is currently a Full Professor of electrical engineering with the Department of Energy, Politecnico di Milano. She is also the Director of the Solar Tech Laboratory (SolarTechLAB) and the Laboratory of MicroGrids (MG$^2$LAB), Politecnico di Milano. She is a Senior Member of the IEEE Power and Energy Society and a member of the IEEE Working Group Distributed Resources Modeling and Analysis.

**EMANUELE OGLIARI** (Member, IEEE) received the M.Sc. degree in electrical engineering and the Ph.D. degree in electrical engineering from Politecnico di Milano, Italy, in 2016. He is currently an Associate Professor with the Department of Energy, Politecnico di Milano, Milan, Italy, where he teaches electrical engineering and photovoltaic-based systems. He is a Staff Member of the SolarTechLAB and the Laboratory of MicroGrids (MG$^2$LAB), Politecnico di Milano.

Open Access funding provided by 'Politecnico di Milano' within the CRUI CARE Agreement